Diffuse Groundwater Discharge Dominates Terrestrial Dissolved Inorganic Carbon Export and CO_2 Evasion From a Semiarid Headwater Stream

Chuan Wang[1], Yueqing Xie[1,2,*], Shaoda Liu[3], James L. McCallum[4], Qing Li[5], and Jichun Wu[1,*]

[1]Ministry of Education Key Laboratory of Surficial Geochemistry, School of Earth Sciences and Engineering, Nanjing University, Nanjing, China

[2]National Centre for Groundwater Research and Training, College of Science and Engineering, Flinders University, Adelaide, South Australia, Australia

[3]Yale School of Forestry and Environmental Studies, Yale University, New Haven, Connecticut, USA

[4]School of Earth Sciences, University of Western Australia, Perth, Western Australia, Australia

[5]State Key Laboratory of Marine Environment Science, College of Ocean & Earth Sciences, Xiamen University, Xiamen, China

[*]Corresponding author: Yueqing Xie (yxie@nju.edu.cn)

Jichun Wu (jcwu@nju.edu.cn)

Key Points:

- Diffuse groundwater discharge controlled terrestrial dissolved inorganic carbon export to the stream.
- A large portion of dissolved CO_2 was transformed into HCO_3^- immediately after entering the stream.
- Semiarid headwater stream CO_2 evasion was driven by carbon transfer, but limited by carbon supply.

Abstract

Groundwater discharge to headwater streams and concomitant terrestrial dissolved inorganic carbon (DIC) export play a significant role in headwater stream CO_2 evasion. However, previous studies rarely examined diffuse groundwater discharge and its impact on headwater stream CO_2 evasion, thereby lacking the understanding of the role of diffuse groundwater discharge in terrestrial DIC export and stream CO_2 evasion. This study quantified diffuse groundwater discharge along a 43 km semiarid headwater stream by combining hydraulic, isotopic (radon-222) and chemical (electrical conductivity) approaches, and estimated the reach-level CO_2 budgets of the stream. Reach-scale water and mass balance modeling yielded highly variable diffuse groundwater discharge rates (n = 16, range: 1.08-7.80 m^2/d, mean ± 1 sd: 4.57 ± 1.81 m^2/d). Groundwater was supersaturated with CO_2 at all sites, with strongly variable CO_2 partial pressure (pCO_2) and DIC concentrations at 1,223-27,349 μatm and 30-119 mg/L, respectively. Diffuse groundwater discharge dominated terrestrial DIC export to the stream (12-111 g C m^{-2} d^{-1}, normalized to water surface area). A portion of groundwater dissolved CO_2 transported to the stream was emitted to the atmosphere with evasion rates varying at 0.62-3.18 g C m^{-2} d^{-1}. However, most dissolved CO_2 was transformed into HCO_3^- through carbonate buffering because of the regulation of carbonate equilibrium. Overall, the stream CO_2 evasion was driven by carbon transfer but limited by carbon supply. This study provides a bottom-up perspective to understand terrestrial DIC export and stream CO_2 evasion in arid and semiarid areas.

45 # 1. Introduction

46 CO_2 evasion from streams and rivers to the atmosphere is a significant process in the global
47 carbon cycle (Battin et al., 2009; Butman and Raymond, 2011; Duvert et al., 2018; Marx et al.,
48 2017; Raymond et al., 2013; Wehrli, 2013). The average partial pressure of carbon dioxide
49 (pCO_2) of global streams and rivers is estimated at 3,100 μatm compared with the atmospheric
50 pCO_2 of approximately 390 μatm. This large difference in pCO_2 results in the common
51 phenomenon of CO_2 supersaturation in the rivers and streams (Marx et al., 2017; Raymond et al.,
52 2013). Consequently, global streams and rivers emit a considerable amount of CO_2 to the
53 atmosphere with the rate estimated at approximately 2.58 petagrams of carbon (Pg C) per year
54 (Marx et al., 2017; Raymond et al., 2013; Sawakuchi et al., 2017). Among all streams and rivers,
55 headwater streams are hotspots, contributing 36% (i.e. 0.93 Pg C yr^{-1}) of the total CO_2 evasion,
56 which is disproportional to their catchment sizes (Marx et al., 2017; Raymond et al., 2013). This
57 significant contribution from the headwater streams is attributed to several factors including a
58 large number of the headwater streams (Marx et al., 2017), high CO_2 concentrations (Butman
59 and Raymond, 2011; Duvert et al., 2018; Horgby et al., 2019; Johnson et al., 2008; Leith et al.,
60 2015; Lupon et al., 2019; Öquist et al., 2009; Winterdahl et al., 2016), and high gas transfer
61 velocities (Liu and Raymond, 2018; Raymond et al., 2013).

62 Continuous CO_2 evasion from streams and rivers is usually derived from two carbon
63 sources, including internal production by microbial mineralization of dissolved organic carbon
64 (DOC), and external input of terrestrial CO_2 (Hotchkiss et al., 2015; Marx et al., 2017). The
65 internal production plays an important role in larger rivers, whereas the external input is essential
66 to continuously sustain CO_2 evasion from small streams, particularly in headwater streams

(Hotchkiss et al., 2015). As reported by several studies in the headwater streams, groundwater pCO_2 is typically 1-2 orders of magnitude higher than stream pCO_2 (Deirmendjian and Abril, 2018; Hope et al., 2004; Johnson et al., 2008; Rasilo et al., 2017). After CO_2-rich groundwater discharges to streams, most dissolved CO_2 (CO_2^*, similarly hereinafter) is emitted to the atmosphere over a short distance downstream (Duvert et al., 2018; Johnson et al., 2008; Öquist et al., 2009). Although these studies have improved our understanding of groundwater contribution to terrestrial carbon export and stream CO_2 evasion, it is hardly possible to upscale their results from local scales to regional scales because of the unknown spatial variability of groundwater carbon input. Some studies have attempted to quantify CO_2 evasion at the regional scale, but utilized only a limited number of groundwater measurements to represent groundwater contribution with an inherent assumption of relatively weak spatial variability of groundwater carbon input (Duvert et al., 2018; Duvert et al., 2019; Leith et al., 2015; Lupon et al., 2019; Öquist et al., 2009). However, the degree of the spatial variability of the groundwater carbon input is still unclear. This knowledge gap undermines our ability to upscale headwater stream CO_2 evasion to larger spatial scales.

Groundwater discharge plays a crucial role in transporting terrestrial carbon to streams and sustaining stream CO_2 evasion (Duvert et al., 2018; Horgby et al., 2019; Lupon et al., 2019; Marx et al., 2017; Winterdahl et al., 2016). Previous stream CO_2 evasion studies have largely concentrated on springs (focused groundwater discharge) where flow rates and CO_2 concentrations are measurable (Duvert et al., 2018; Johnson et al., 2008; Lupon et al., 2019). However, in many systems, groundwater discharge is known to occur through an entire stream diffusively and at rates that are difficult to be measured directly. This diffuse groundwater discharge has been frequently examined in many streams and rivers at varying length scales and

has been found to be strongly variable due to variable hydraulic gradients and riverbed permeability (Cook et al., 2006; Xie et al., 2016). Therefore, accurate quantitative analysis of CO_2 evasion from headwater streams at large scales requires reliable estimation of diffuse groundwater discharge rates.

Here, we longitudinally surveyed a 43 km semiarid headwater stream (Hailiutu River) where stream flow was mostly maintained by groundwater discharge throughout a year (Yang et al., 2012; 2014). We quantified the groundwater discharge by combining hydraulic, isotopic and chemical methods, and then estimated the stream carbon budget at the corresponding resolution. Through the constrained water and mass balances, we attempted to explore (i) the main driver of terrestrial carbon export in a semiarid headwater stream; (ii) the main driver of stream CO_2 evasion; and (iii) the role of diffuse groundwater discharge in terrestrial carbon export and release.

2. Data and Methods

2.1. Site description

Our study was conducted in the Hailiutu River catchment, located in Yulin City, Shanxi Province, semiarid northern China. The total area of this catchment is around 2,645 km^2, and the surface elevation of this catchment ranges from 1,486 m above sea level (m.a.s.l.) in the northwest to 1,009 m in the southeast (Figure 1). The land surface is mainly covered by undulating sand dunes and xeric shrubland (Yang et al., 2012). The regional aquifer is composed of the Holocene Maowusu sand dunes (thickness: 0-30 m) underlain by the upper Pleistocene Shalawusu sandstone (thickness: 5-90 m) (Yang et al., 2014). This catchment is controlled by

111 semiarid continental climate with low precipitation (340 mm yr^{-1}) and high potential
112 evapotranspiration (2,184 mm yr^{-1}) (Yang et al., 2012). The majority of the precipitation occurs
113 from June to September every year.

114 The Hailiutu River and its tributary, the Bulang River, are the two major streams in this
115 catchment (Figure 1). The Hailiutu River is formed by two small streams in the northwest of our
116 study area and extends all the way to the Hanjiamao Village (4 km above the confluence with the
117 Wuding River, Figure 1). It is a perennial second-order stream with the annual mean stream flow
118 rate of 2.41 m^3/s at the gauging station close to the catchment exit (2001-2007) (Yang et al.,
119 2012). The Hailiutu River water eventually flows into the Wuding River, a major tributary along
120 the middle reach of the Yellow River (Yang et al., 2012). The studied section of the Hailiutu
121 River is approximately 43 km in length.

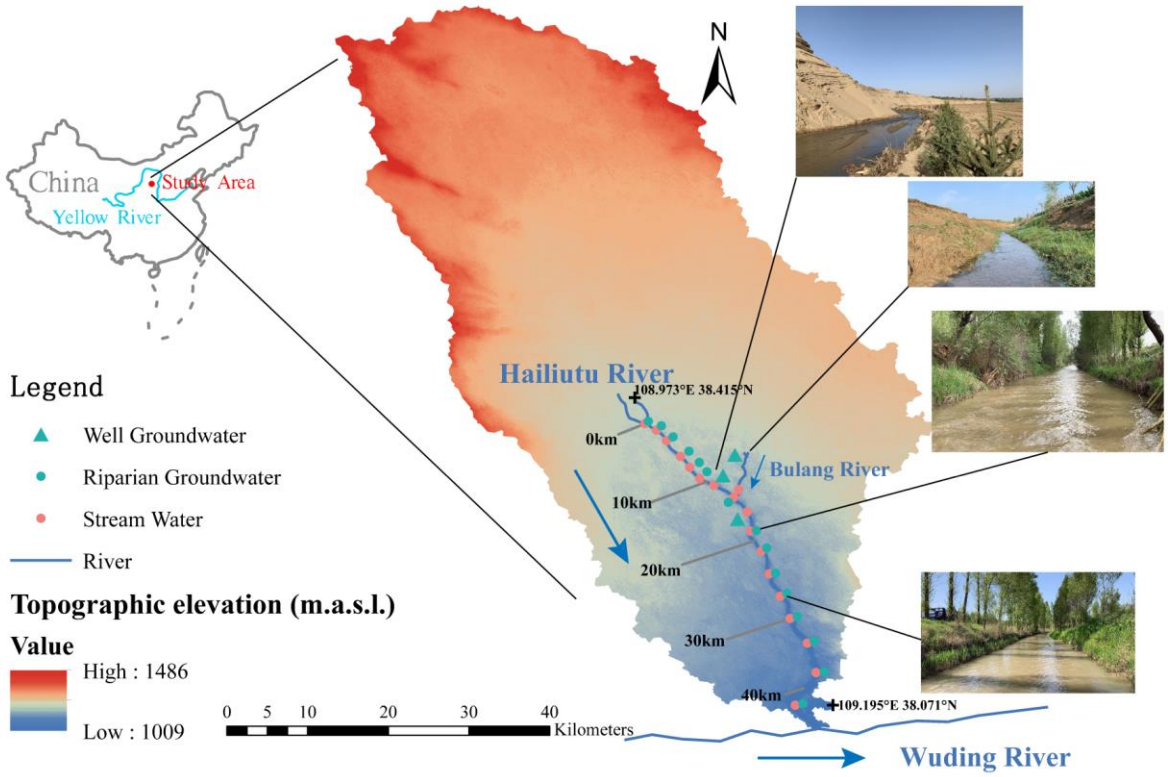

122

Figure 1. Geographic location of the study area and sampling sites along the Hailiutu River.

2.2. Field survey and laboratory analyses

Our field survey was conducted between 9 and 14 May 2019 (dry season) when the stream was mainly sustained by groundwater discharge. We longitudinally surveyed the stream water and its adjacent groundwater at an average interval of 2.6 km (Figure 1). For groundwater sampling, we excavated holes (approximately 0.5 m wide and 0.4-0.6 m deep) at the riverbank and sampled the fresh groundwater within a short period of excavation (15 samples). Samples were also collected from domestic wells located within 1 km of the stream (2 samples, Figure 1). These wells were screened in the sand aquifer to depths between 15 and 135 m below ground level.

We quantified groundwater discharge to the Hailiutu River by combining differential flow gauging and the mass balance modeling of radon-222 (^{222}Rn) and electrical conductivity (EC). Flow gauging was undertaken at each sampling location by dividing the stream transect into intervals of approximately 0.5 m. The flow velocity of each 0.5 m section was measured using a flow meter (accuracy: ±1.5%, Jiangsu Nanshui Water Technology Company, China) with the one-point method. The total stream flow rate was obtained by summing the flow rate of all the sections (flow velocity multiplied by the cross-sectional area). ^{222}Rn activities in both the stream and the groundwater were obtained via the RAD7 detector coupled with the RAD H_2O Accessory (Durridge Company, USA). The stream and the groundwater excavations were sampled by submerging and sealing a 250 mL glass vial underwater. Domestic groundwater wells were purged with a minimum of three bore volumes removed and sampled after groundwater temperature, pH and EC had stabilized. EC in both the stream and the groundwater

was measured with the HACH HQ40d multiparameter probe (accuracy: ±0.5%, HACH Company, USA).

Both the stream water and groundwater were also measured for dissolved oxygen, pH and temperature in the field through the HACH HQ40d multiparameter probe. Their alkalinity was titrated through HACH Digital Titrator (accuracy: ±1%). pCO_2 and DIC concentrations were calculated by field measured pH, temperature and alkalinity (Supplementary information, SI, Text S1). In addition to the field direct measurements, water samples were also collected for analyzing cations, anions, DOC and $\delta^{13}C_{DIC}$ in the laboratory. All the water samples were filtered through 0.45 μm membrane filters and acidified by adding HCl if used for cation analysis. The cations and anions were analyzed through ICP-OES and ion chromatography, respectively, at the Key Laboratory of Surficial Geochemistry of the Ministry of Education, Nanjing University. DOC was analyzed through a TOC analyzer (SHIMADZU TOC-L, Japan) at the School of the Environment, Nanjing University. The $\delta^{13}C_{DIC}$ was measured through the Gasbench and MAT252 (Thermo Fisher Scientific, USA) at the State Key Laboratory for Mineral Deposits Research, Nanjing University.

2.3. Reach-scale water and mass balance modeling

Reach-scale groundwater discharge to the Hailiutu River was estimated by modeling the stream water balance and the mass balances of ^{222}Rn and EC simultaneously (Cook, 2013; Cook et al., 2006). The stream water balance is given by

$$\frac{\partial Q}{\partial x} = I + Tri - Ew \quad (1)$$

where Q is the stream flow rate (m^3/d), x is the distance in the direction of flow (m), I is the groundwater discharge per unit length (m^2/d), Tri is the tributary inflow rate per unit length (m^2/d), E is the evaporation rate (m/d) , and w is the stream width (m). Tri is equal to the tributary flux (positive, i.e. Bulang River flux) or irrigation diversion flux (negative, we found three irrigation diversion points) divided by the length between two adjacent stream measurement points.

The environmental tracer ^{222}Rn has been used frequently to quantify groundwater discharge to surface water (Cook, 2013; Cook et al., 2003; Cook et al., 2006; Hofmann et al., 2011; Xie et al., 2016). ^{222}Rn is a radioactive noble gas with a half-life of 3.8 days. It is a decay product of uranium series isotopes. Given the extensive existence of uranium in aquifer sediment, ^{222}Rn is produced continuously in groundwater. Once groundwater discharges to the stream, ^{222}Rn activity is affected by several factors including gas exchange with the atmosphere, radioactive decay and dispersive mixing. The mass balance of ^{222}Rn is given by the following equation (Cook, 2013; Cook et al., 2003; Cook et al., 2006)

$$\frac{\partial(QC)}{\partial x} = IC_{gw} + Tri \cdot C_{Tri} - kwC - \lambda dwC + F_{hypor} \quad (2)$$

where C, C_{gw}, and C_{Tri} are the ^{222}Rn activities (Bq/L) of the stream, the adjacent groundwater, and the tributary, respectively. C_{Tri} equals C for irrigation diversion. k is the ^{222}Rn gas transfer velocity (m/d), λ is the radioactive constant of ^{222}Rn (0.18 d^{-1}), d is the stream depth (m), and F_{hypor} is the net flux of ^{222}Rn from hyporheic zone into stream. The first two terms on the right side of the equation represent mass fluxes due to groundwater discharge and tributary inflow,

185 respectively. The third and fourth terms on the right side represent ^{222}Rn loss rates due to gas
186 exchange with the atmosphere and radioactive decay, respectively. The last term is hyporheic
187 flow related mass flux. Cook et al. (2006) derived the expression of the net flux of ^{222}Rn from
188 hyporheic zone into stream (F_{hypor})

189 $$F_{hypor} = \frac{wh\theta(\gamma - \lambda C)}{1 + \lambda t_h} \quad (3)$$

190 where h (m), θ (dimensionless), γ (Bq/L/day), and t_h (d) are the mean depth, the porosity, the
191 ^{222}Rn production rate, and the mean water residence time within the hyporheic zone, respectively.
192 Noting that $\frac{\partial(QC)}{\partial x} = C\frac{\partial Q}{\partial x} + Q\frac{\partial C}{\partial x}$, and substituting this together with Equation (1) and (3) into
193 (2) results in the following equation

194 $$Q\frac{\partial C}{\partial x} = I\left(C_{gw} - C\right) + Tri\left(C_{Tri} - C\right) + EwC - kwC - \lambda dwC + \frac{wh\theta(\gamma - \lambda C)}{1 + \lambda t_h} \quad (4)$$

195 For EC, the k, λ and F_{hypor} are zero as they are only related to ^{222}Rn production and losses.
196 Equation (4) then becomes

197 $$Q\frac{\partial C}{\partial x} = I\left(C_{gw} - C\right) + Tri\left(C_{Tri} - C\right) + EwC \quad (5)$$

198 Groundwater discharge was quantified by solving Equation (1), (4) and (5) simultaneously,
199 with an explicit finite difference method. A grid size of 10 m was used, resulting in a total of
200 4,298 cells given the modeled stream length of 42.98 km. We utilized the DiffeRential Evolution
201 Adaptive Metropolis scheme (“DREAM” algorithm) (Vrugt et al., 2009), which is based on an

evolutionary Markov chain Monte-Carlo (MCMC) approach to calibrate the groundwater discharge and other model parameters (i.e., k, h, γ and t_h). The DREAM algorithm runs multiple Markov chains simultaneously for multi-modal search problems and improves the efficiency of MCMC simulation significantly (Vrugt et al., 2009). This method has been effectively used to model stream tracer tests (Knapp and Cirpka, 2017; McCallum et al., 2020; Roche et al., 2019). The DREAM algorithm works by generating multiple Markov chains to sample the parameter space by selecting combinations of parameters that produce a better fit to the observed values (also known as the likelihood). The likelihood function used in this study was defined as

$$Likelihood = -\left(\sum_{i=1}^{17} \left(\frac{Q_{modeled} - Q_{measured}}{Q_{error}} \right)^2 + \sum_{i=1}^{17} \left(\frac{Rn_{modeled} - Rn_{measured}}{Rn_{error}} \right)^2 + \sum_{i=1}^{17} \left(\frac{EC_{modeled} - EC_{measured}}{EC_{error}} \right)^2 \right) \quad (6)$$

where $Q_{modeled}$, $Rn_{modeled}$, and $EC_{modeled}$ are the modeled stream flow rate, ^{222}Rn activity, and EC derived from the MCMC simulation, respectively. $Q_{measured}$, $Rn_{measured}$, and $EC_{measured}$ are the field measured stream flow rate, ^{222}Rn activity, and EC, respectively. Q_{error}, Rn_{error}, and EC_{error} are the errors of stream flow rate, ^{222}Rn activity, and EC, respectively.

In the DREAM algorithm, new proposals are generated first using combinations of other chains. If these proposals produce a higher likelihood, the proposal is accepted. If the new likelihood is lower, the chains accept the proposal conditional on a transition probability (a transition to a slightly worse likelihood is more probable than a transition to a much lower likelihood). At each level, either the proposed values (if transition conditions are met) or the

current values form a set of samples. Each of these samples is treated equally, and the resulting statistics of all the sampled parameters sets encapsulate the range of plausible values or uncertainty.

2.4. Reach-scale carbon budgeting

Based on the reach-scale water balance, we established a reach-scale CO_2 budget to explore the contributions of external input, internal production and carbonate buffering process to the stream CO_2 evasion. For a representative stream reach, we assumed that the stream was in steady state (i.e., the inputs and outputs are equal)

$$F_{up}^{CO_2} + F_{gw}^{CO_2} + F_{Tri}^{CO_2} + F_{m}^{CO_2} = F_{down}^{CO_2} + F_{air}^{CO_2} + F_{b}^{CO_2} \quad (7)$$

where $F_{up}^{CO_2}$, $F_{gw}^{CO_2}$, $F_{Tri}^{CO_2}$, and $F_{m}^{CO_2}$ are the upstream CO_2 input, the groundwater CO_2 input, the tributary CO_2 input, the net internal CO_2 production (DOC mineralization minus photosynthesis), respectively. $F_{down}^{CO_2}$, $F_{air}^{CO_2}$, and $F_{b}^{CO_2}$ are the downstream CO_2 output, the stream CO_2 evasion rate, and the CO_2 loss through carbonate buffering (positive value means CO_2^* transformed into HCO_3^-, and negative value means HCO_3^- transformed into CO_2^*), respectively. Note that all the mass fluxes in Equation (7) are normalized to the water surface area of the given stream reach and expressed in g C m^{-2} d^{-1}. $F_{up}^{CO_2}$, $F_{gw}^{CO_2}$, $F_{Tri}^{CO_2}$, and $F_{down}^{CO_2}$ are determined by multiplying the CO_2 concentrations and the water fluxes derived from the water balance. $F_{m}^{CO_2}$ is derived from the reach-scale mass balance of DOC. $F_{air}^{CO_2}$ is estimated by Fick's Law. Finally, $F_{b}^{CO_2}$ can be calculated from Equation (7).

241 In the water column, DOC can be degraded to CO_2^*, sustaining the stream CO_2
242 oversaturation and CO_2 evasion to the atmosphere. CO_2^* can also be conversely consumed by
243 photosynthesis. Here, we utilized a reach-scale DOC mass balance to estimate $F_m^{CO_2}$

244 $$F_m^{CO_2} = F_{up}^{DOC} + F_{gw}^{DOC} + F_{Tri}^{DOC} - F_{down}^{DOC} \quad (8)$$

245 where F_{up}^{DOC}, F_{gw}^{DOC}, F_{Tri}^{DOC}, and F_{down}^{DOC} are the upstream DOC input, the groundwater DOC
246 input, the tributary DOC input, and the downstream DOC output, respectively. Likewise, these
247 carbon fluxes are also quantified by multiplying the corresponding DOC concentrations and the
248 water fluxes derived from the water balance.

249 $F_{air}^{CO_2}$ is estimated by Fick's Law and given below

250 $$F_{air}^{CO_2} = \left(pCO_{2\,aq} - pCO_{2\,air} \right) \times K_H \times K_{CO_2} \times 12 \div 1000 \quad (9)$$

251 where $pCO_{2\,aq}$ and $pCO_{2\,air}$ are the CO_2 partial pressure in the stream and the air (μatm),
252 respectively. We assumed that the atmospheric pCO_2 was 390 μatm. K_H and K_{CO_2} are the
253 temperature-dependent Henry's Law constant (mol/L/atm) and the CO_2 gas transfer velocity
254 (m/d).

255 K_H is determined according to the empirical equation from Clark and Fritz (1997)

256 $$-\log_{10}\left(K_H\right) = -7 \times 10^{-5} T^2 + 0.016T + 1.11 \quad (10)$$

257 where T is the temperature of stream water (°C).

258 K_{CO_2} can be determined from the calibrated ^{222}Rn gas transfer velocity (k, m/d) derived
259 from the reach-scale water and mass balance modeling (Raymond et al., 2012)

260 $$K_{CO_2} = k\left(\frac{Sc_{CO_2}}{Sc_{Rn}}\right)^{-0.5} \quad (11)$$

261 where Sc_{CO_2} and Sc_{Rn} are the Schmidt number of CO_2 and ^{222}Rn, respectively. Both Sc_{CO_2} and
262 Sc_{Rn} can be calculated from stream temperature (℃) (Raymond et al., 2012)

263 $$Sc_{CO_2} = 1742 - 91.24T + 2.208T^2 - 0.0219T^3 \quad (12)$$

264 $$Sc_{Rn} = 2939 - 173.87T + 4.532T^2 - 0.0468T^3 \quad (13)$$

265 Previous studies found that carbonate buffering can significantly impact stream CO_2
266 evasion by shifting carbonate equilibrium, particularly in high alkalinity streams and rivers
267 (Duvert et al., 2019; Stets et al., 2017). Oversaturated CO_2 in the stream can be either emitted to
268 the atmosphere or transformed into HCO_3^-. Relevant chemical reactions are given below

269 $$CO_2(g) = CO_2(aq) \quad (14)$$

270 $$CO_2(aq) + H_2O = H_2CO_3 = H^+ + HCO_3^- = 2H^+ + CO_3^{2-} \quad (15)$$

271 $$Ca^{2+} + 2HCO_3^- = CaCO_3\downarrow + CO_2^* + H_2O \quad (16)$$

272 Equation (7) can be rearranged to examine the impact of the carbon buffering process to the
273 stream CO_2 pool as follows

$$F_b^{CO_2} = F_{up}^{CO_2} + F_{gw}^{CO_2} + F_{Tri}^{CO_2} + F_m^{CO_2} - F_{down}^{CO_2} - F_{air}^{CO_2} \quad (17)$$

2.5. Hydrogeochemical modeling

We modeled carbonate buffering process after groundwater discharged to the stream through the PHREEQC simulation program (Parkhurst and Appelo, 2013). The mean water temperature, pH, Ca^{2+}, Mg^{2+} and alkalinity of our groundwater samples were assigned as the initial model parameters, then we modeled the re-equilibrium processes between the groundwater and the air for different pCO_2 values and calculated the corresponding calcite saturation (Ion Activity Product / Solubility Product Constant of calcite, IAP/K calcite, similarly hereinafter). Through the change of calcite saturation, we can explore the shift in carbonate equilibriums.

2.6. Uncertainty and statistical analysis

Uncertainty analysis was based on the results of the MCMC simulation. For the variables estimated in the MCMC simulation (i.e., I, k, h, γ and t_h), we treated the 16th-84th percentiles of the model outputted ranges as their uncertainty bounds. For the other variables including $F_{gw}^{CO_2}$, $F_m^{CO_2}$ and $F_b^{CO_2}$, their uncertainty bounds were determined according to the uncertainty bounds of I. The uncertainty of $F_{air}^{CO_2}$ were based on the k uncertainty.

Furthermore, we used one-way analysis of variance (ANOVA test) to compare the carbon concentration differences between the stream and the groundwater, and different carbon budget components at the significance level of $p < 0.05$.

3. Results

3.1. Longitudinal patterns of stream flow and groundwater discharge

Field measured values for reach-scale water and mass balance modeling are listed in SI Table S1, and the spatial variations in Q, ^{222}Rn activities and EC are depicted in Figure 2a-c, respectively. Differential flow gauging shows that stream velocity ranged between 0.190 and 1.156 m/s and Q increased continuously from 0.283 m^3/s at the upstream end of the studied reach to 2.093 m^3/s at the downstream end, with some fluctuations between 15 and 25 km (Figure 2a). Stream width varies between 3.8 and 11 m, with the mean value of 6.34 m. The stream is relatively shallow (range: 0.11–0.49 m) with a mean depth of 0.25 m.

The stream ^{222}Rn activities were significantly lower than those from the adjacent groundwater (ANOVA, $n = 34$, $F = 481$, $p < 0.0001$). The mean ± 1 standard deviation (similarly hereinafter) of the stream and groundwater ^{222}Rn activities are 0.889 ± 0.236 and 5.082 ± 0.752 Bq/L, respectively. The ^{222}Rn activity along the stream was fluctuating but relatively stable at 0-27 km (0.832-1.150 Bq/L) and decreased from 1.046 at 27 km to 0.322 Bq/L at 43 km (Figure 2b).

The stream EC shows a decreasing trend along the stream (Figure 2c), with the maximum of 994 μs/cm at the upstream end and the minimum of 456 μs/cm at 34 km. The groundwater EC was significantly lower than the stream EC (ANOVA, $n = 34$, $F = 4.58$, $p < 0.05$) and varied between 241 and 679 μs/cm.

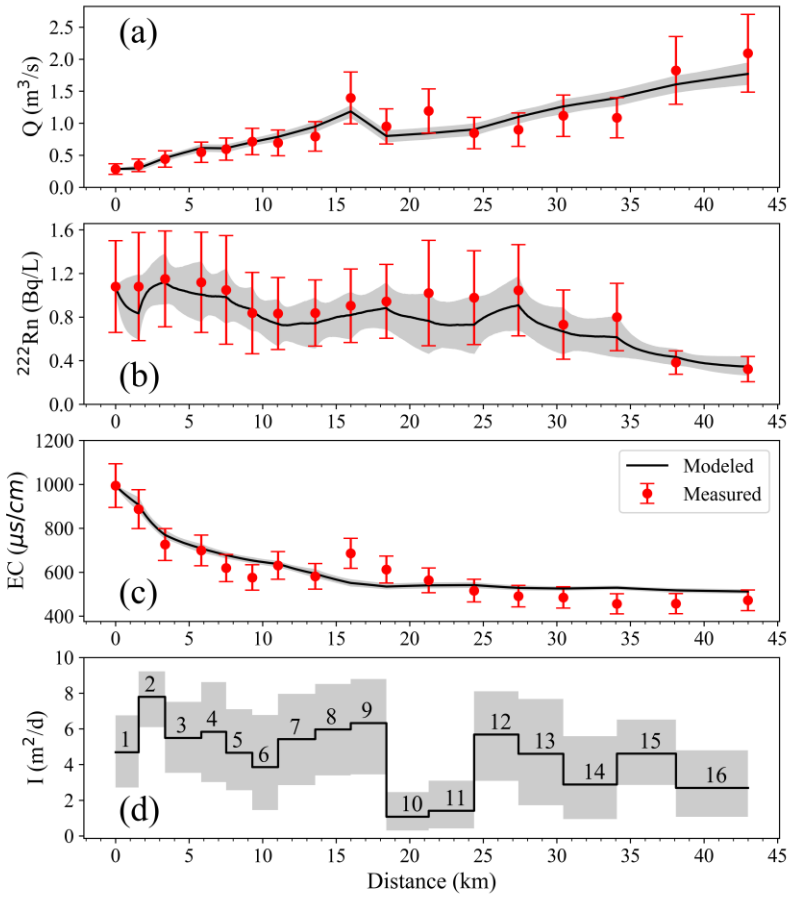

Figure 2. Reach-scale water and mass balance modeling results of (a) stream flow rates (*Q*), (b) ^{222}Rn activities, (c) EC, and the resultant variation in (d) groundwater discharge rates (*I*). The black lines and shaded areas show optimal modeling results (50th percentile) and uncertainty bounds (16th-84th percentile) derived from the MCMC simulation, respectively. The red dots are the field measured values and the error bars show the relevant uncertainties. The stream reach numbers are annotated above the line segments in (d).

Model parameters are defined in SI Table S2. Parameters E, θ and λ were assumed to be constant. For each stream reach, the upstream and downstream sampling sites were used to calculate w, d, and C_{gw}. There are three small irrigation canals along the Hailiutu River where we did not measure the ^{222}Rn activities and EC. We assumed that the ^{222}Rn activities and EC in the irrigation canals were the same as those of the nearest stream sampling site ($C_{Tri}=C$). This assumption is reasonable as these values were only used to account for water and mass losses

from the study stream. Q_0, C_0 at the first sampling site (Hailiutu-01 in SI Table S1) were utilized as the boundary conditions of the longitudinal water and mass balance model.

Errors are required in the likelihood function for the MCMC simulation. We measured the Hailiutu-01, Hailiutu-02, Hailiutu-03 and Hailiutu-09 stream flow rates twice. The average relative error at these four sites were utilized as the potential error for all stream flow rates (29%). The error of the ^{222}Rn activities were the 2-sigma uncertainty derived from the CAPTURE software (https://durridge.com/). An error of 10% was assumed for EC to cover potential measurement and analytical errors as used by McCallum et al. (2012).

Modeled groundwater discharge rates (I) are shown in Figure 2d, while other calibrated parameters (k, h, γ and t_h) are depicted in SI Figure S1. The reach-scale water and mass balance modeling results (black lines in Figure 2a-c) agree with the field measurements reasonably well (for the most optimal case, the likelihood is -21.56, the root mean square errors are 0.18 m^3/s, 0.126 Bq/L and 55 μs/cm for Q, ^{222}Rn activities and EC, respectively). The modeling results indicate that the groundwater discharge occurred along the entire stream other than concentrating on some local areas, and I varied between 1.08 and 7.80 m^2/d with the mean ± 1 standard deviation at 4.57 ± 1.81 m^2/d. The highest and lowest I occurred at Reach 2 and Reach 10, respectively. The uncertainty of I is approximately 2 m^2/d (shaded area in Figure 2d).

3.2. Longitudinal patterns of carbon concentrations in stream and groundwater

Stream DIC concentrations show a slightly decreasing trend from 62 mg/L at the upstream end to 43 mg/L at the downstream end (Figure 3a). In comparison, groundwater DIC concentrations (66 ± 24 mg/L) fluctuated more strongly than those of stream water (48 ± 5 mg/L)

(Figure 3). Notably, DIC was the main carbon species in both the stream and the adjacent groundwater, because the DIC concentrations were approximately nine times higher than DOC concentrations in both the stream and groundwater (ANOVA, n = 34, F = 1012 and 97, respectively, both p values < 0.0001). Stream and groundwater DOC concentrations were relatively constant along the stream with the values at 5 ± 1 and 7 ± 3 mg/L, respectively. Both the stream and the adjacent groundwater were supersaturated with CO_2 with pCO_2 at 719 ± 168 μatm and 9,343 ± 7,050 μatm, respectively, when compared with the average atmospheric pCO_2 of 390 μatm. Furthermore, groundwater pCO_2 correlates well with groundwater DIC (Figure 3b, $R^2 = 0.91$, $p < 0.0001$).

Overall, the DIC, DOC and CO_2 concentrations in the groundwater were significantly higher than those in the stream (Figure 4, ANOVA, n = 34, F = 9.01, 6.70 and 25.42, respectively, all p values < 0.05). Particularly, pCO_2 in the groundwater was an order of magnitude higher than that in the stream with the mean values at 9,343 and 719 μatm, respectively. We also found that DIC concentrations and pCO_2 in the riparian groundwater were higher than those in the groundwater from the wells (SI Table S3).

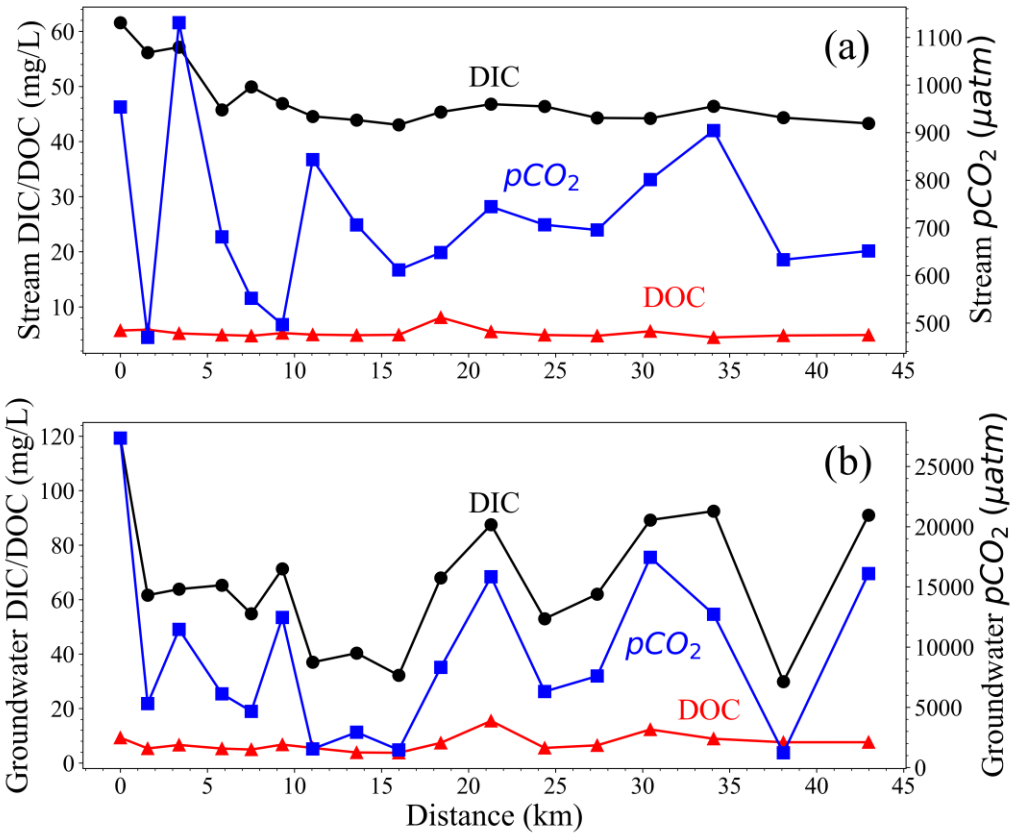

359

360 **Figure 3.** Spatial variations in DIC, DOC and pCO_2 along (a) the Hailiutu River and (b) the adjacent
361 groundwater.

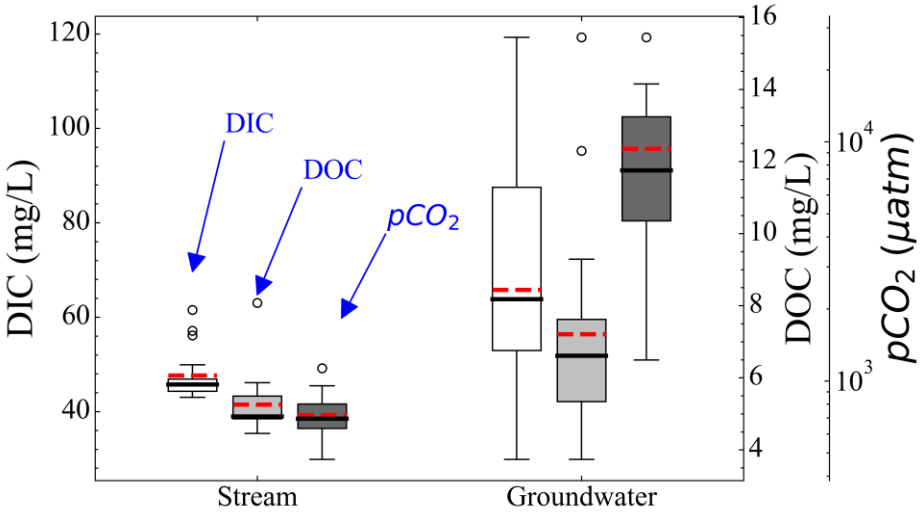

362

Figure 4. The comparison of DIC, DOC and pCO_2 in the Hailiutu River (n = 17) to those in the adjacent groundwater (n = 17). Boxes indicate median and interquartile range, whiskers show the maximum and minimum values, dots are outliers from the whiskers, and red dashed lines represent mean values.

3.3. Hydrogeochemical processes after groundwater discharges to stream

pCO_2 and IAP/K (calcite) in the groundwater are higher and lower than the corresponding values in the stream, respectively (Figure 5, ANOVA, n = 34, F = 25.42 and 60.46, respectively, both p values < 0.001). The stream was generally supersaturated with calcite with the IAP/K (calcite) of 11.45 ± 4.99 (Range: 6.31~27.54). The modeled results (blue dashed curve in Figure 5) indicate that the calcite saturation (IAP/K) increased significantly after the CO_2-rich groundwater discharged to the stream.

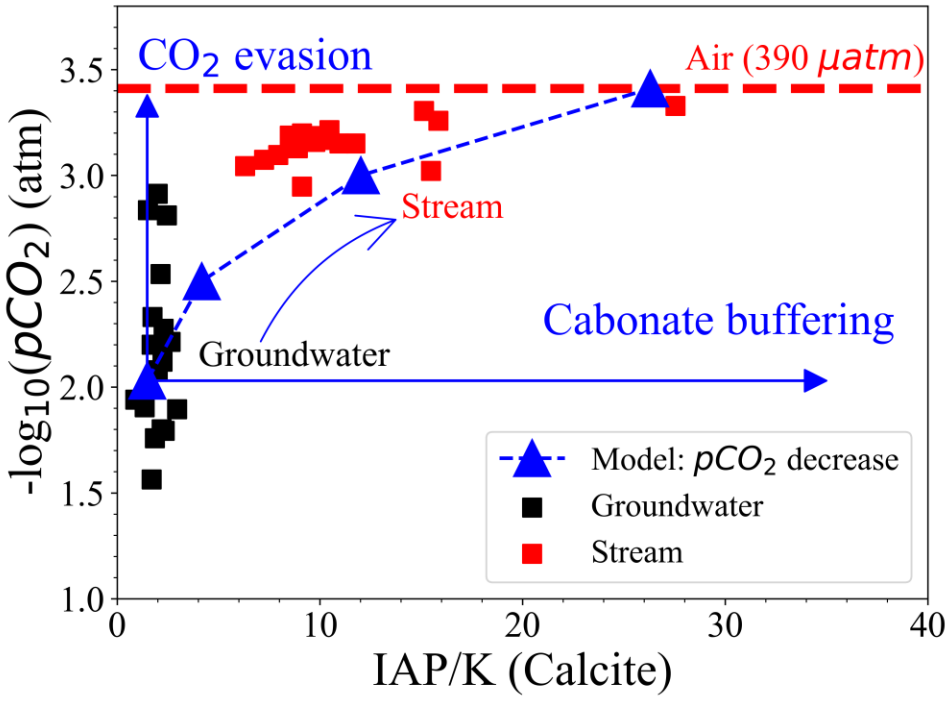

Figure 5. The hydrogeochemical processes after the groundwater (black squares) discharged to the stream (red squares). IAP/K(Calcite) was derived from the PHREEQC modeling. The upward arrow indicates the CO_2 evasion process, while the rightward arrow shows the carbonate buffering process (i.e., CO_2^* was transformed

into HCO_3^-), thereby causing the supersaturation of calcite. The blue triangles are the modeled results when groundwater re-equilibrates with the air of $-\log_{10}(pCO_2)$ (atm) at 2.03 (i.e., 9,343 μatm, the average pCO_2 of the 17 groundwater samples in our study), 2.5, 3.0, 3.41 (i.e., 390 μatm, the atmospheric pCO_2), respectively. The model parameters used in the PHREEQC simulation are defined in SI Table S4.

3.4. Terrestrial carbon export and stream CO_2 evasion

The measured data for quantifying the reach-scale carbon budget are listed in SI Table S3, and these results are depicted in Figure 6-8. The comparison between external and internal CO_2 contributions indicates that the external CO_2 input was higher than the net internal CO_2 production ($F_{gw}^{CO_2}$: 3.73 ± 2.52 g C m^{-2} d^{-1}, $F_m^{CO_2}$: 1.08 ± 4.66 g C m^{-2} d^{-1}, Figure 6). It should be noted that the net internal CO_2 production at all the stream sections except Reaches 5, 8, 9 and 13 made positive contribution to the stream CO_2 balance (Figure 6a). Since DIC is the main carbon species in both the groundwater and the stream as discussed above, the terrestrial carbon export is primarily in the form of DIC. The reach-scale terrestrial DIC export (F_{gw}^{DIC}, the product of the groundwater DIC concentrations and *I*) was 48.78 ± 28.78 g C m^{-2} d^{-1}, and varied between 12.20 and 111.13 g C m^{-2} d^{-1} (Figure 7a). *I* at Reach 2 was the highest (Figure 2d), and F_{gw}^{DIC} was also the highest (Figure 7a). Conversely, where *I* was limited (e.g., Reaches 10 and 11), F_{gw}^{DIC} was also constrained (Figure 7a).

Notably, both the stream and the groundwater were high in pH (8.50 ± 0.10 and 7.60 ± 0.25, SI Table S3) and alkalinity (3.98 ± 0.46 and 5.04 ± 1.71 meq/L, SI Table S3). Thus, carbonate buffering plays a significant role in regulating the stream CO_2 pool in our study (Duvert et al., 2019; Stets et al., 2017). The CO_2 mass balance results show that most reaches (except Reaches 8 and 9) had positive $F_b^{CO_2}$ values (Figure 7b). This indicates that most CO_2^* was transformed

399 into HCO_3^- after the CO_2-rich groundwater discharged to the stream and the carbonate buffering
400 inhibited the stream CO2 evasion. Furthermore, we found $F_b^{CO_2}$ was positively correlated with
401 $F_m^{CO_2}$ (SI Figure S2), and $F_b^{CO_2}$ is generally higher than $F_{air}^{CO_2}$ with the average values of 3.15 and
402 1.39 g C m^{-2} d^{-1} (Figure 7b and 7c), respectively.

403 Our model calculation based on Equation (9) shows that $F_{air}^{CO_2}$ varied strongly along the
404 stream (1.39 ± 0.73 g C m^{-2} d^{-1}, range: 0.62~3.18 g C m^{-2} d^{-1}, model B in Figure 8). $F_{air}^{CO_2}$ was
405 also derived from an empirical model (model A in Figure 8, SI Text S2) with the values at 1.79 ±
406 1.25 g C m^{-2} d^{-1} (range: 0.36~4.16 g C m^{-2} d^{-1}). This comparison indicates that our model for
407 calculating $F_{air}^{CO_2}$ performed reasonably well (Figure 8b). Since our K_{CO_2} values were calibrated
408 through the water and mass balance modeling, our $F_{air}^{CO_2}$ values are likely to be better than those
409 empirically derived values.

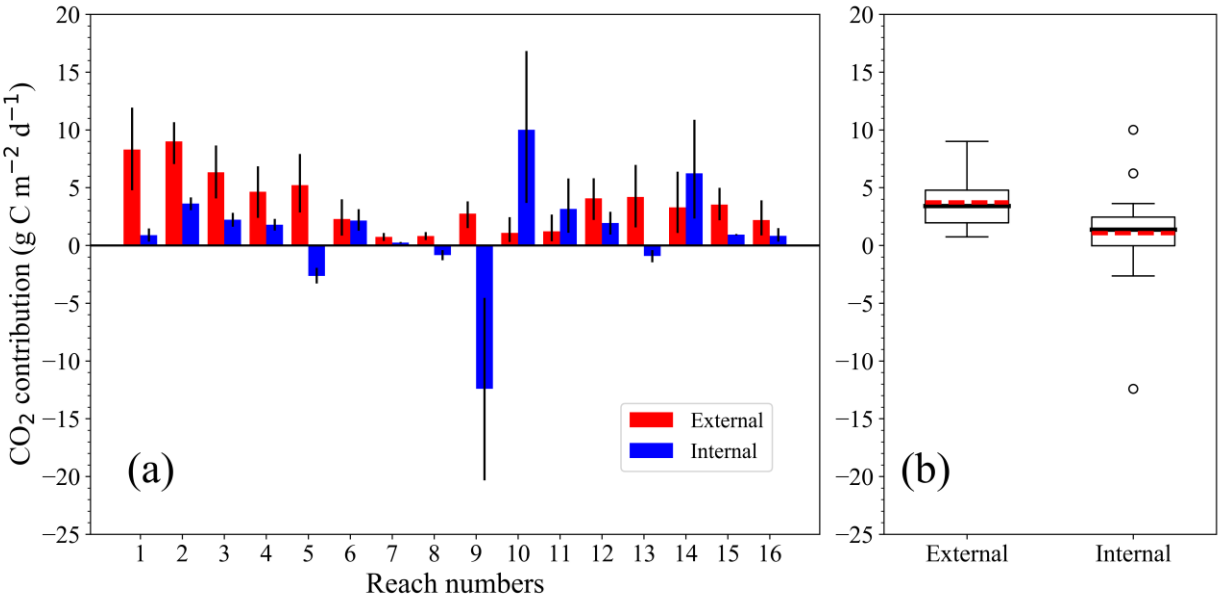

410

411 **Figure 6.** (a) The reach-scale comparison and (b) the corresponding boxplot comparison of external CO_2 input
412 ($F_{gw}^{CO_2}$)to net internal CO_2 production ($F_m^{CO_2}$). Error bars in (a) represent the uncertainties caused by
413 groundwater discharge. Boxes in (b) indicate median and interquartile range, whiskers show the maximum and
414 minimum values, dots are outliers from the whiskers, and red dashed lines represent mean values.

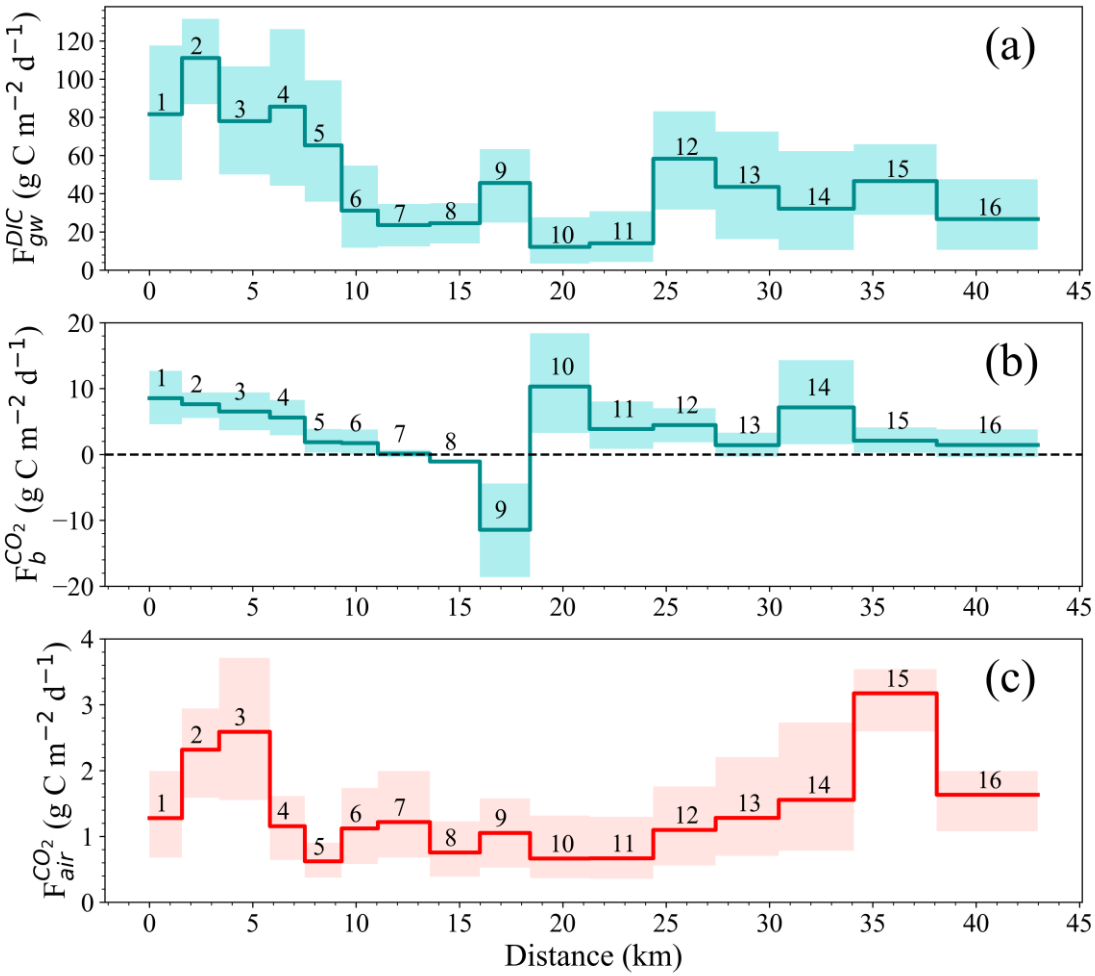

415

416 **Figure 7.** The spatial variation in (a) terrestrial DIC export via diffuse groundwater discharge (F_{gw}^{DIC}), (b)
417 carbonate buffering transformation within the stream ($F_b^{CO_2}$) (positive values mean that CO_2^* is transformed
418 into HCO_3^-, and vice versa), and (c) stream CO_2 evasion rate ($F_{air}^{CO_2}$) along the stream. The shaded areas
419 around each line represent the uncertainty bounds. Numbers above line segments are stream reach numbers.

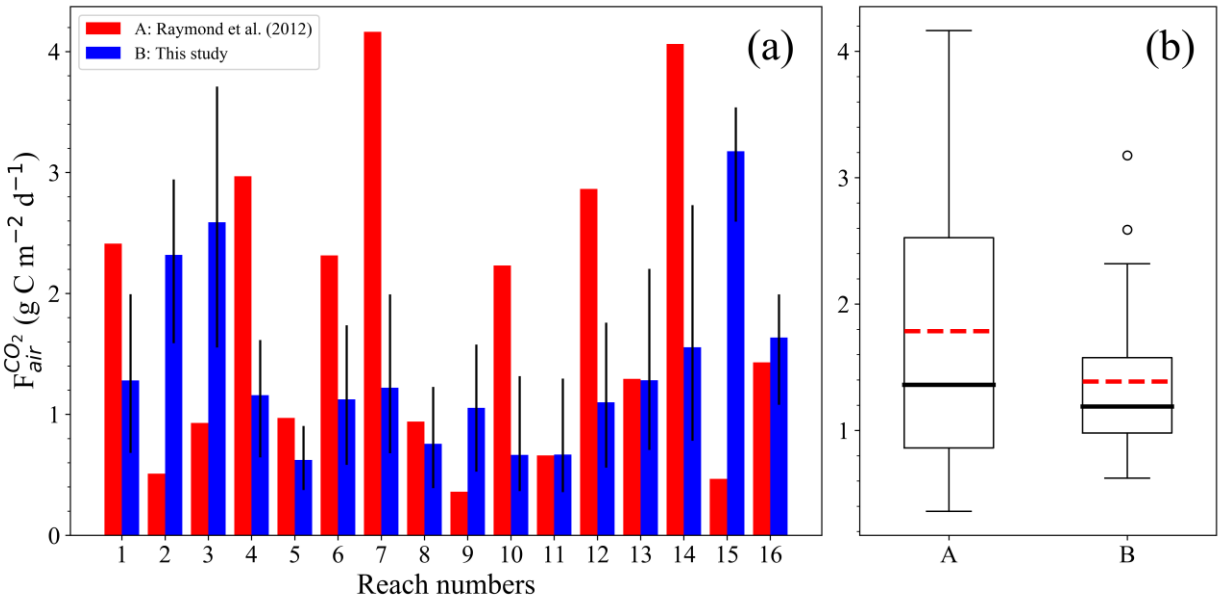

Figure 8. (a) Comparison of reach-scale stream CO_2 evasion rates between an empirical model (model A, Equation (7) in Raymond et al. (2012), SI Text S2) and our study (model B). (b) The statistical comparison between model A and model B. Error bars in (a) represent the uncertainty caused by the uncertainty of ^{222}Rn gas transfer velocity. Boxes in (b) indicate the medians and interquartile ranges, whiskers show the maximum and minimum values, dots are outliers from the whiskers, and the red dashed lines represent the mean values.

3.5. Potential drivers for terrestrial carbon export and release

Both the terrestrial DIC export and the stream CO_2 evasion can be controlled by either carbon transfer (i.e., groundwater discharge rate and CO_2 gas transfer velocity, Zone A in Figure 9) or carbon supply (i.e., groundwater DIC concentration and stream pCO_2, Zone C in Figure 9). The reaches located at Zone B in Figure 9 are hotspots for carbon fluxes and driven by both the transfer and the supply, whereas the reaches located in Zone D are limited by both the transfer and the supply and so are not important for carbon fluxes. In our study, most reaches are hotspots (located at Zone B in Figure 9a) for terrestrial DIC export except Reaches 10 and 11 (limited by groundwater discharge, Figure 2d). Stream CO_2 evasion rates are mainly located close to the

435 threshold for dividing Zone A and Zone B in Figure 9b, indicating that the carbon fluxes are
436 driven by the transfer but limited by the supply.

437 Terrestrial DIC export to headwater streams is mainly controlled by groundwater discharge
438 and groundwater DIC concentrations (Horgby et al., 2019; Leith et al., 2015; Lupon et al., 2019;
439 Öquist et al., 2009; Öquist et al., 2014). In our study, we found that the terrestrial DIC export is
440 positively correlated with the groundwater discharge, but no significant correlation between the
441 terrestrial DIC export and the groundwater DIC concentration (Figure 10a and 10c). In
442 comparison, the stream CO_2 evasion is positively correlated with both the CO_2 gas transfer
443 velocity and stream pCO_2, with the former more significant than the latter (Figure 10b and 10d).

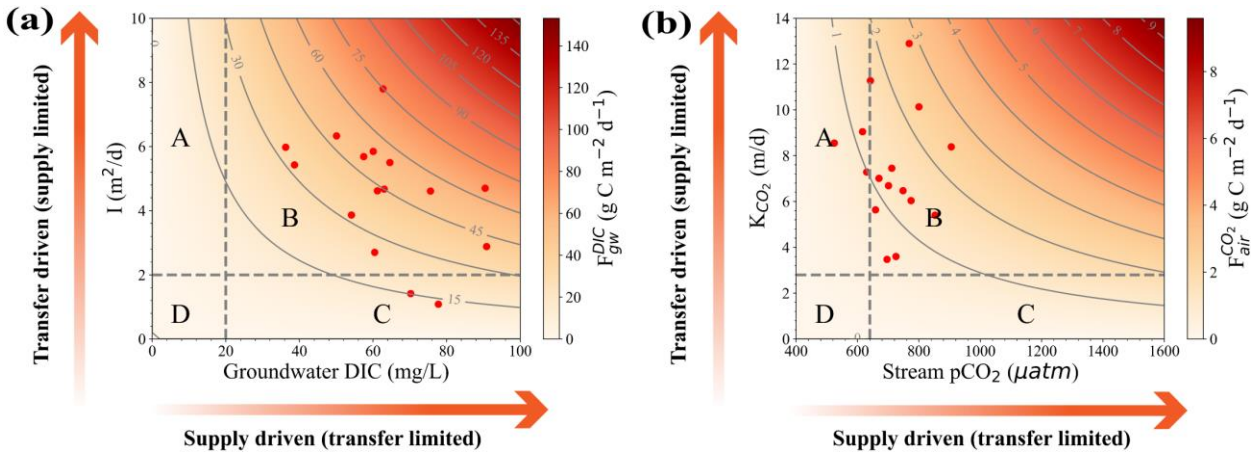

444

445 **Figure 9.** The main control factors on (a) terrestrial DIC export (F_{gw}^{DIC}) and (b) stream CO_2 evasion ($F_{air}^{CO_2}$).
446 We utilized the mean reach distance (2.69 km), surface area (17,571 m^2), and stream water temperature
447 (14.4 ℃) in our study to estimate the isolines (grey solid lines) for terrestrial DIC export and stream CO_2
448 evasion. The red dots represent the 16 stream reaches. The carbon fluxes can be driven by either carbon
449 transfer (A), carbon supply (C), or both (B). Hotspots of carbon fluxes (B) can then occur when the supply is
450 sufficient and the transfer is fast. Conversely, both the supply and the transfer limited zones (D) are less
451 significant for carbon fluxes. The threshold values (grey dashed lines) for dividing these zones (A-D) are
452 somewhat subjective and based on plausible minimum values of carbon fluxes at hotspots identified through

the literature review (Butman and Raymond, 2011; Liu and Raymond, 2018; Marx et al., 2017; McCallum et al., 2012; Raymond et al., 2013).

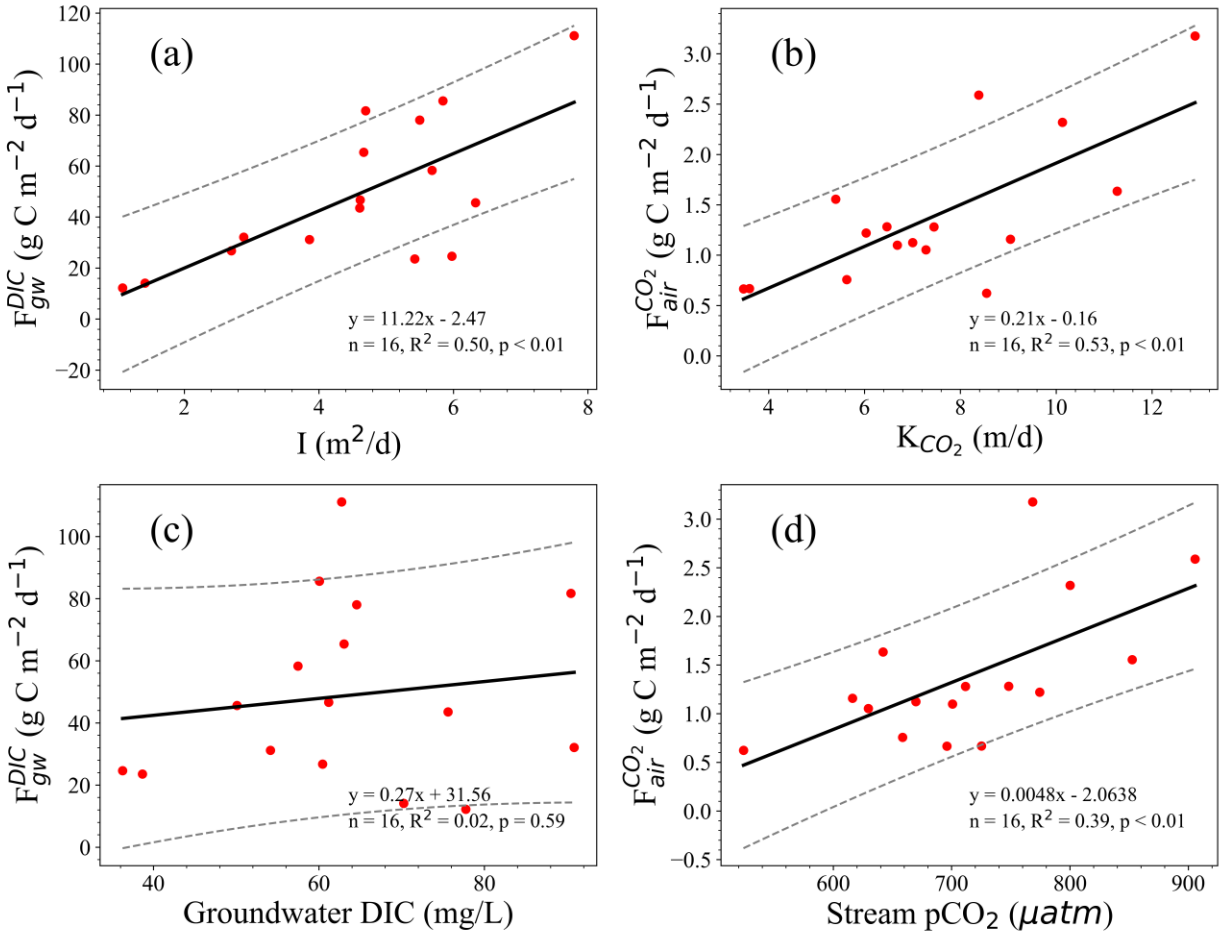

Figure 10. Correlations between (a) terrestrial DIC export (F_{gw}^{DIC}) and groundwater discharge (*I*), (b) stream CO_2 evasion ($F_{air}^{CO_2}$) and CO_2 gas transfer velocity (K_{CO_2}), (c) terrestrial DIC export and groundwater DIC concentration, and (d) stream CO_2 evasion and stream pCO_2. Black lines are the linear regression results, while the grey dashed lines are the 10% and 90% confidence intervals.

4. Discussion

4.1. Diffuse groundwater discharge as a significant driver for terrestrial DIC export

Since our field survey was conducted in the dry season, the steady increase in the stream flow rate was largely attributed to the diffuse groundwater discharge other than the precipitation nor the surface water inflow. This has been supported by the presence of the relatively high stream ^{222}Rn activities and the gradual decline in the stream EC along the stream. In our studied catchment, the stream bank and streambed were composed of highly conductive and homogeneous sand (Yang et al., 2012; 2014). Focused groundwater discharge via preferential flow paths is unlikely to occur in such an environment. Rather, the groundwater discharge is more likely to occur in a diffusive pattern along the stream (Duvert et al., 2018; Lupon et al., 2019).

Previous studies highlighted the control of focused groundwater discharge on stream CO_2 evasion, but failed to demonstrate the contribution from diffuse groundwater discharge (Duvert et al., 2018; Johnson et al., 2008; Lupon et al., 2019). In this study, we found that the diffuse groundwater discharge not only maintained the streamflow, but also continuously exported a considerable amount of terrestrial carbon to the stream, in particular the terrestrial DIC. As the diffuse groundwater discharge is widely existent (Cook et al., 2003; Cook et al., 2006; McCallum et al., 2012; Xie et al., 2016), it is expected to be the main driver for the terrestrial DIC export in not only our headwater stream but also many other headwater streams.

4.2. Terrestrial DIC export as the major carbon source for streams

As demonstrated by previous studies, supersaturated CO_2^* in streams and rivers is mainly derived from external input (i.e., terrestrial DIC export) or internal metabolism (Hotchkiss et al., 2015). Here, we found that the terrestrial DIC export via the diffuse groundwater discharge played a more significant role in contributing CO_2^* to the studied headwater stream compared

with the internal metabolism, which is consistent with existing studies (Duvert et al., 2018; Hotchkiss et al., 2015; Öquist et al., 2009; Winterdahl et al., 2016). More importantly, our study indicates that the riparian zone had a stronger impact on the terrestrial DIC export and stream CO_2 evasion because of the higher DIC and CO_2 concentrations in the riparian groundwater than those in the groundwater from the domestic wells (Hope et al., 2004; Leith et al., 2015; Lupon et al., 2019; Vidon et al., 2010). In semiarid headwater streams, the riparian zone allows for better vegetation growth than areas that are relatively far from the streams. Therefore, soil respiration is more active in the riparian zone than in the rest of the catchment, causing the higher CO_2 concentrations (Hope et al., 2004; Leith et al., 2015).

This finding was also supported by groundwater $\delta^{13}C_{DIC}$ values (-11.90 ± 1.98 ‰, see SI Table S5), which fall in the potential $\delta^{13}C_{DIC}$ range for C4 plants (corn in our case) grown in the riparian zone (Clark and Fritz, 1997). Furthermore, our $\delta^{13}C_{DIC}$ data also suggest that terrestrial DIC export is the main carbon source of stream DIC pool. After terrestrial DIC was exported to the stream, the CO_2 gas exchange between the stream and atmosphere and the internal metabolism resulted in more positive $\delta^{13}C_{DIC}$ values in stream than in groundwater (ANOVA, $n = 34$, $F = 8.64$, $p < 0.01$) (Deirmendjian and Abril, 2018).

4.3. Stream CO_2 evasion was driven by carbon transfer but limited by carbon supply

The terrestrial CO_2 export via the diffuse groundwater discharge directly sustained the stream CO_2 evasion. However, considering the high pH and high alkalinity setting in our study area, most of the terrestrial DIC exported to the stream were in the form of HCO_3^-. Thus, the transformation between CO_2^* and HCO_3^- (carbonate buffering) can also indirectly enhance or limit the stream CO_2 evasion by regulating stream CO_2 pool (conceptual model in Figure 11),

506 especially in high alkalinity streams (Duvert et al., 2019; Stets et al., 2017). Our CO_2 mass
507 balance results indicate that the carbonate buffering caused most CO_2^* to be transformed into
508 HCO_3^- after the CO_2-rich groundwater discharged to the stream, thereby increasing the calcite
509 saturation of the stream water (Figure 5) (Jacobson and Usdowski, 1975; Lorah and Herman,
510 1988; Lu et al., 2000). Although most reaches are the hotspots for the terrestrial DIC export
511 (Figure 9a), most CO_2^* loss occurred through the carbonate buffering, causing the limited carbon
512 supply for the stream CO_2 evasion. The limited CO2 evasion was supported by very close mean
513 $\delta^{13}C_{DIC}$ values of stream water and groundwater (-10.46 ‰ and -11.90 ‰, respectively, SI Table
514 S5). This CO_2 loss mechanism is attributed to the high alkalinity and pH setting in groundwater
515 and stream. This diffuse groundwater discharge pattern is different from previous studies where
516 most CO2 was emitted to the atmosphere due to focused groundwater discharge (Duvert et al.,
517 2018; Johnson et al., 2008). Thus, the stream CO_2 evasion in our study catchment was driven by
518 the carbon transfer but limited by the carbon supply (most reaches have high CO_2 gas transfer
519 velocity but relatively low stream pCO_2).

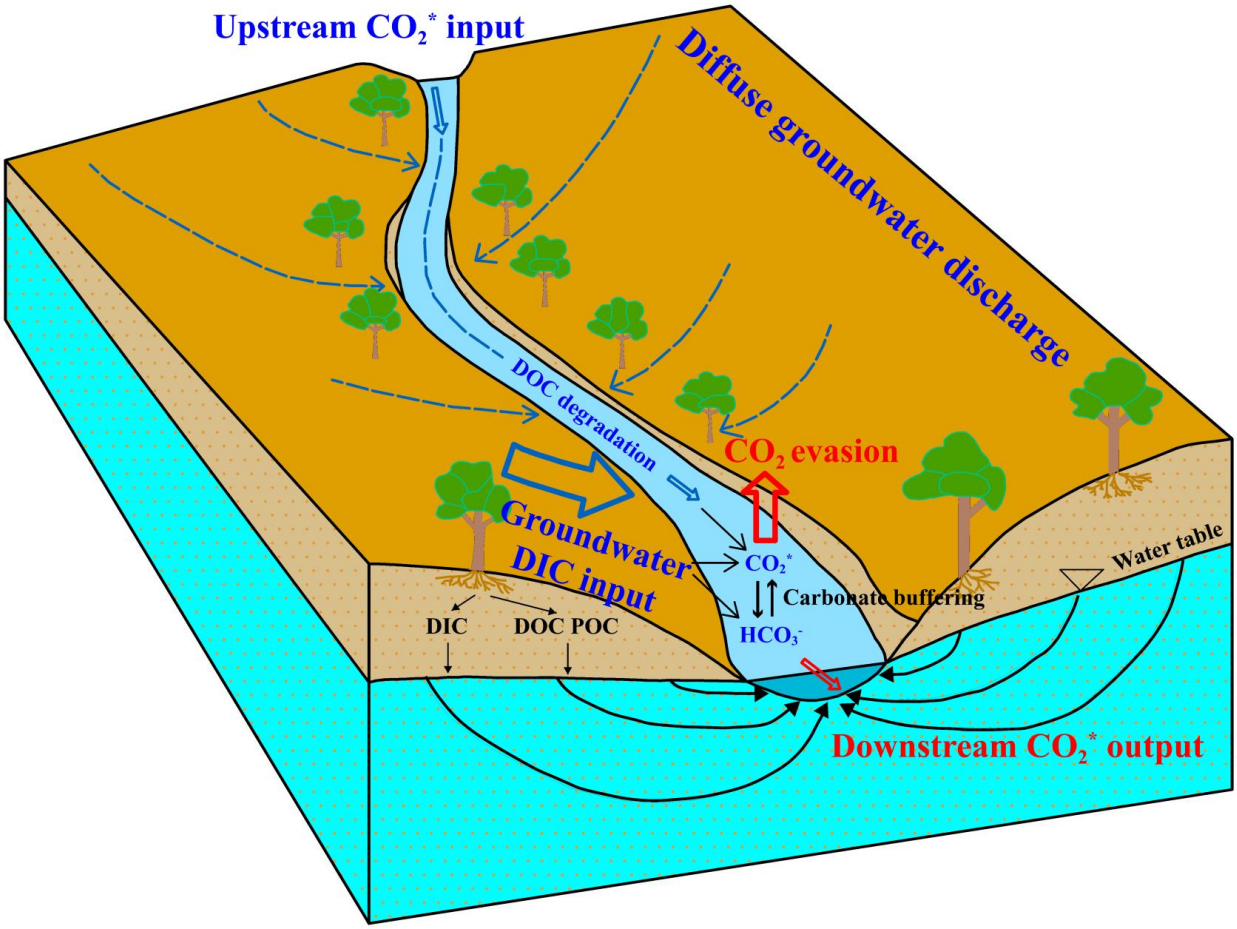

Figure 11. The conceptual model demonstrates that diffuse groundwater discharge dominates terrestrial DIC export, and carbonate buffering process regulates stream CO_2 pool through transformation between CO_2^* and HCO_3^-. This carbonate buffering process can either enhance (i.e., HCO_3^- transformed into CO_2) or limit (i.e., CO_2 transformed into HCO_3^-) stream CO_2 evasion. In our study stream, the carbonate buffering largely limited the stream CO_2 evasion.

4.4. Implication for CO_2 evasion from semiarid headwater streams

Previous studies quantifying headwater stream CO_2 evasion focused mostly on peatland streams (Billett and Harvey, 2013; Hope et al., 2001; Long et al., 2015) and forested streams (Aho and Raymond, 2019; Jones and Mulholland, 1998; Marx et al., 2018; Öquist et al., 2009; Wallin et al., 2013) due to high internal production in these environments. However, headwater

streams in arid and semiarid regions are likely to be a significant "transfer station" for terrestrial carbon export and release to the atmosphere because of their close connection with terrestrial ecosystem through diffuse groundwater discharge. Our reach-scale carbon budget results indicate that stream CO_2 evasion rates (0.62-3.18 g C m^{-2} d^{-1} in our study) could be comparable to the average CO_2 efflux of conterminous US streams (2.42-10.98 g C m^{-2} d^{-1}) (Butman and Raymond, 2011). Comparison in headwater stream CO_2 evasion rates between our study, peatland and forested headwater streams suggests that headwater stream CO_2 evasion from arid and semiarid regions may be as important as that from humid regions (SI Table S6).

Former studies pointed out semiarid headwater streams may also be hotspots for CO_2 evasion (Gómez-Gener et al., 2015; Schiller et al., 2014). Our CO_2 evasion rates are higher than those reported in these studies (Mediterranean rivers, 0.20-2.63 and 0.49-1.15 g C m^{-2} d^{-1}, respectively). We attributed the higher stream CO_2 evasion rates in our study to the greater diffuse groundwater discharge rates and higher CO_2 gas transfer velocities (transfer driven). As our survey was conducted during the dry season, our results may represent the lower bound of the Hailiutu River CO_2 evasion rates. Larger CO_2 evasion rates are expected to occur when groundwater discharge is higher during the wet season.

5. Conclusions

In this study, we discovered that headwater streams in arid and semiarid areas are significant sources of CO_2 to the atmosphere. These understudied streams received a considerable amount of dissolved CO_2 from terrestrial ecosystems via diffuse groundwater discharge. Interestingly, a large portion of dissolved CO_2 was not directly and quickly emitted to the atmosphere, but transformed into HCO_3^- through carbonate buffering. The stream CO_2

553 evasion was driven by fast carbon transfer processes between terrestrial ecosystems, stream and
554 atmosphere, but limited by relatively small carbon supply in stream due to the inhibition of
555 carbonate buffering. To the best of our knowledge, previous studies seldom integrated the vital
556 contribution of terrestrial carbon export via diffuse groundwater discharge to headwater stream
557 carbon budget, which may underestimate headwater stream CO_2 evasion rates (Duvert et al.,
558 2018; Hotchkiss et al., 2015; Johnson et al., 2008; Lupon et al., 2019; Marx et al., 2017; Öquist
559 et al., 2009). Our analysis highlights the importance of the diffuse groundwater discharge on
560 terrestrial DIC export and stream CO_2 evasion at the regional scale.

561 Acknowledgments

562 The authors confirm that there is no conflict of interest. Additional supporting information
563 can be found in the supporting information (SI). All research data used in this study are available
564 and can be found at figshare repository (https://doi.org/10.6084/m9.figshare.12295769.v1). This
565 research was supported by the National Natural Science Foundation of China (No. 41972246)
566 and the Fundamental Research Funds for the Central Universities (No. 020614380088).

567 References

568 Aho, K. S., and Raymond, P. A. (2019). Differential response of greenhouse gas evasion to
569 storms in forested and wetland streams. *Journal of Geophysical Research: Biogeosciences*,
570 *124*(3), 649-662.

571 Battin, T. J., Luyssaert, S., Kaplan, L. A., Aufdenkampe, A. K., Richter, A., and Tranvik, L. J.
572 (2009). The boundless carbon cycle. *Nature Geoscience*, *2*(1), 598-600.

573 Billett, M. F., and Harvey, F. H. (2013). Measurements of CO_2 and CH_4 evasion from UK
574 peatland headwater streams. *Biogeochem.*, *114*(1-3), 165-181.

575 Butman, D., and Raymond, P. A. (2011). Significant efflux of carbon dioxide from streams and
576 rivers in the United States. *Nature Geoscience*, *4*(12), 839-842.

Clark, I. D., and Fritz, P. (1997), *Environmental Isotopes in Hydrogeology*, CRC Press, Taylor & Francis Group, New York.

Cook, P. G. (2013). Estimating groundwater discharge to rivers from river chemistry surveys. *Hydrological Processes*, *27*(25), 3694-3707.

Cook, P. G., Favreau, G., Dighton, J. C., and Tickell, S. (2003). Determining natural groundwater influx to a tropical river using radon, chlorofluorocarbons and ionic environmental tracers. *Journal of Hydrology*, *277*(1-2), 74-88.

Cook, P. G., Lamontagne, S., Berhane, D., and Clark, J. F. (2006). Quantifying groundwater discharge to Cockburn River, southeastern Australia, using dissolved gas tracers ^{222}Rn and SF_6. *Water Resources Research*, *42*(10).

Deirmendjian, L., and Abril, G. (2018). Carbon dioxide degassing at the groundwater-stream-atmosphere interface: isotopic equilibration and hydrological mass balance in a sandy watershed. *Journal of Hydrology*, *558*, 129-143.

Duvert, C., Butman, D. E., Marx, A., Ribolzi, O., and Hutley, L. B. (2018). CO_2 evasion along streams driven by groundwater inputs and geomorphic controls. *Nature Geoscience*, *11*(11), 813-818.

Duvert, C., Bossa, M., Tyler, K. J., Wynn, J. G., Munksgaard, N. C., Bird, M. I., et al. (2019). Groundwater-derived DIC and carbonate buffering enhance fluvial CO_2 evasion in two Australian tropical rivers. *Journal of Geophysical Research: Biogeosciences*, *124*(2), 312-327.

Gómez-Gener, L., Obrador, B., von Schiller, D., Marcé, R., Casas-Ruiz, J. P., Proia, L., et al. (2015). Hot spots for carbon emissions from Mediterranean fluvial networks during summer drought. *Biogeochemistry*, *125*(3), 409-426.

Hofmann, H., Gilfedder, B. S., and Cartwright, I. (2011). A novel method using a silicone diffusion membrane for continuous ^{222}Rn measurements for the quantification of groundwater discharge to streams and rivers. *Environmental Science & Technology*, *45*(20), 8915-8921.

Hope, D., Palmer, S. M., Billett, M. F., and Dawson, J. J. C. (2001). Carbon dioxide and methane evasion from a temperate peatland stream. *Limnology and Oceanography*, *46*(4), 847-857.

Hope, D., Palmer, S. M., Billett, M. F., and Dawson, J. J. C. (2004). Variations in dissolved CO_2 and CH_4 in a first-order stream and catchment: an investigation of soil–stream linkages. *Hydrological Processes*, *18*(17), 3255-3275.

Horgby, Å., Canadell, M. B., Ulseth, A. J., Vennemann, T. W., and Battin, T. J. (2019). High-resolution spatial sampling identifies groundwater as driver of CO_2 dynamics in an Alpine stream network. *Journal of Geophysical Research: Biogeosciences*, *124*(7), 1961-1976.

Hotchkiss, E. R., Hall Jr, R. O., Sponseller, R. A., Butman, D., Klaminder, J., Laudon, H., et al. (2015). Sources of and processes controlling CO_2 emissions change with the size of streams and rivers. *Nature Geoscience*, *8*, 696-699.

Jacobson, R. L., and Usdowski, E. (1975). Geochemical Controls on a Calcite Precipitating Spring. *Contr. Mineral. Petrol.*, *51*(1), 65-74.

Johnson, M. S., Lehmann, J., Riha, S. J., Krusche, A. V., Richey, J. E., Ometto, J. P. H. B., et al. (2008). CO_2 efflux from Amazonian headwater streams represents a significant fate for deep soil respiration. *Geophysical Research Letters*, *35*(17).

Jones, J. B., and Mulholland, P. J. (1998). Carbon dioxide variation in a hardwood forest stream: An integrative measure of whole catchment soil respiration. *Ecosystems*, *1*(2), 183-196.

Knapp, J. L. A., and Cirpka, O. A. (2017). Determination of hyporheic travel time distributions and other parameters from concurrent conservative and reactive tracer tests by local-in-global optimization. *Water Resources Research*, *53*(6), 4984-5001.

Leith, F. I., Dinsmore, K. J., Wallin, M. B., Billett, M. F., Heal, K. V., Laudon, H., et al. (2015). Carbon dioxide transport across the hillslope–riparian–stream continuum in a boreal headwater catchment. *Biogeosciences*, *12*, 1881-1892.

Liu, S., and Raymond, P. A. (2018). Hydrologic controls on pCO_2 and CO_2 efflux in US streams and rivers. *Limnology and Oceanography*, *3*(6), 428-435.

Long, H., Vihermaa, L., Waldron, S., Hoey, T., Quemin, S., and Newton, J. (2015). Hydraulics are a first - order control on CO_2 efflux from fluvial systems. *Journal of Geophysical Research: Biogeosciences*, *120*(10), 1912-1922.

Lorah, M. M., and Herman, J. S. (1988). The Chemical Evolution of a Travertine-Depositing Stream - Geochemical Processes and Mass-Transfer Reactions. *Water Resources Research*, *24*(9), 1541-1552.

Lu, G., Zheng, C., Donahoe, R. J., and Lyons, W. B. (2000). Controlling processes in a $CaCO_3$ precipitating stream in Huanglong Natural Scenic District, Sichuan, China. *Journal of Hydrology*, *230*(1-2), 34-54.

Lupon, A., Denfeld, B. A., Laudon, H., Leach, J., Karlsson, J., and Sponseller, R. A. (2019). Groundwater inflows control patterns and sources of greenhouse gas emissions from streams. *Limnology and Oceanography*, *64*(4), 1545-1557.

Marx, A., Conrad, M., Aizinger, V., Prechtel, A., van Geldern, R., and Barth, J. A. C. (2018). Groundwater data improve modelling of headwater stream CO_2 outgassing with a stable DIC isotope approach. *Biogeosciences*, *15*(10), 3093-3106.

Marx, A., Dusek, J., Jankovec, J., Sanda, M., Vogel, T., van Geldern, R., et al. (2017). A review of CO_2 and associated carbon dynamics in headwater streams: A global perspective. *Reviews of Geophysics*, *55*(2), 560-585.

McCallum, J. L., Cook, P. G., Berhane, D., Rumpf, C., and McMahon, G. A. (2012). Quantifying groundwater flows to streams using differential flow gaugings and water chemistry. *Journal of Hydrology*, *416-417*, 118-132.

McCallum, J. L., Höhne, A., Schaper, J. L., Shanafield, M., Banks, E. W., Posselt, M., et al. (2020). A Numerical Stream Transport Modeling Approach Including Multiple Conceptualizations of Hyporheic Exchange and Spatial Variability to Assess Contaminant Removal. *Water Resources Research*, *56*(3).

Öquist, M. G., Wallin, M., Seibert, J., Bishop, K., and Laudon, H. (2009). Dissolved Inorganic Carbon Export Across the Soil/Stream Interface and Its Fate in a Boreal Headwater Stream. *Environmental Science & Technology*, *43*(19), 7364-7369.

Öquist, M. G., Bishop, K., Grelle, A., Klemedtsson, L., Köhler, S. J., Laudon, H., et al. (2014). The Full Annual Carbon Balance of Boreal Forests Is Highly Sensitive to Precipitation. *Environmental Science & Technology Letter*, *1*(7), 315-319.

Parkhurst, D. L., and Appelo, C. A. J. (2013), *Description of input and examples for PHREEQC version 3: a computer program for speciation, batch-reaction, one-dimensional transport, and inverse geochemical calculations*, 497 pp., U.S. Geological Survey Techniques and Methods.

Rasilo, T., Hutchins, R. H. S., Ruiz-González, C., and del Giorgio, P. A. (2017). Transport and transformation of soil-derived CO_2, CH_4 and DOC sustain CO_2 supersaturation in small boreal streams. *Science of The Total Environment*, *579*, 902-912.

Raymond, P. A., Zappa, C. J., Butman, D., Bott, T. L., Potter, J., Mulholland, P., et al. (2012). Scaling the gas transfer velocity and hydraulic geometry in streams and small rivers. *Limnology and Oceanography: Fluids and Environments*, *2*(1), 41-53.

Raymond, P. A., Hartmann, J., Lauerwald, R., Sobek, S., McDonald, C., Hoover, M., et al. (2013). Global carbon dioxide emissions from inland waters. *Nature*, *503*(7476), 355-359.

Roche, K. R., Shogren, A. J., Aubeneau, A., Tank, J. L., and Bolster, D. (2019). Modeling benthic versus hyporheic nutrient uptake in unshaded streams with varying substrates. *Journal of Geophysical Research: Biogeosciences*, *124*(2), 367-383.

Sawakuchi, H. O., Neu, V., Ward, N. D., Barros, M. d. L. C., Valerio, A. M., Gagne-Maynard, W., et al. (2017). Carbon Dioxide Emissions along the Lower Amazon River. *Frontiers in Marine Science*, *4*(76).

Schiller, D. v., Marcé, R., Obrador, B., Gómez-Gener, L., Casas-Ruiz, J. P., Acuña, V., et al. (2014). Carbon dioxide emissions from dry watercourses. *Inland Waters*, *4*(4), 377-382.

Stets, E. G., Butman, D., McDonald, C. P., Stackpoole, S. M., DeGrandpre, M. D., and Striegl, R. G. (2017). Carbonate buffering and metabolic controls on carbon dioxide in rivers. *Global Biogeochemical Cycles*, *31*(4), 663-677.

Vidon, P., Allan, C., Burns, D., Duval, T. P., Gurwick, N., Inamdar, S., et al. (2010). Hot Spots and Hot Moments in Riparian Zones: Potential for Improved Water Quality Management1. *Journal of The American Water Resources Association*, *46*(2), 278-298.

684 Vrugt, J. A., Braak, C. J. F., Diks, C. G. H., Robinson, B. A., Hyman, J. M., and Higdon, D.
685 (2009). Accelerating Markov Chain Monte Carlo Simulation by Differential Evolution with
686 Self-Adaptive Randomized Subspace Sampling. *International Journal of Nonlinear Sciences*
687 *and Numerical Simulation*, *10*(3), 273-290.

688 Wallin, M. B., Grabs, T., Buffam, I., Laudon, H., Ågren, A., Öquist, M. G., et al. (2013).
689 Evasion of CO_2 from streams – The dominant component of the carbon export through the
690 aquatic conduit in a boreal landscape. *Global Change Biology*, *19*(3), 785-797.

691 Wehrli, B. (2013). Biogeochemistry: Conduits of the carbon cycle. *Nature*, *503*(7476), 346-347.

692 Winterdahl, M., Wallin, M. B., Karlsen, R. H., Laudon, H., Öquist, M., and Lyon, S. W. (2016).
693 Decoupling of carbon dioxide and dissolved organic carbon in boreal headwater streams.
694 *Journal of Geophysical Research: Biogeosciences*, *121*(10), 2630-2651.

695 Xie, Y., Cook, P. G., Shanafield, M., Simmons, C. T., and Zheng, C. (2016). Uncertainty of
696 natural tracer methods for quantifying river–aquifer interaction in a large river. *Journal of*
697 *Hydrology*, *535*, 135-147.

698 Yang, Z., Zhou, Y., Wenninger, J., and Uhlenbrook, S. (2012). The causes of flow regime shifts
699 in the semi-arid Hailiutu River, Northwest China. *Hydrology and Earth System Sciences*, *16*,
700 87-103.

701 Yang, Z., Zhou, Y., Wenninger, J., and Uhlenbrook, S. (2014). A multi-method approach to
702 quantify groundwater/surface water-interactions in the semi-arid Hailiutu River basin,
703 northwest China. *Hydrogeology Journal*, *22*(3), 527-541.

704